Characterizing the polarization aberrations in widefield fluorescence microscopy using phase retrieval

R. Gutiérrez-Cuevas[1, 2, *]

[1] *Aix Marseille Univ, CNRS, Centrale Marseille, Institut Fresnel, UMR 7249, 13397 Marseille Cedex 20, France*
[2] *Institut Langevin, ESPCI Paris, Université PSL, CNRS, 75005 Paris, France*

(Dated: September 26, 2022)

Here we present the theory and the different strategies for retrieving the pupil of in fluorescence microscopy where the effects of birefringence play an important role. We also study the effect of separating the signal into different polarization channels.

I. INTRO

General intro about fluorescence microscopy, SMOLM and PSF engineering. Finish by saying something all=ong th elines of: However, any aberration or misalignment in the system can affect the final shape of the PSFs and thus lead to an inaccurate estimate of the parameters.

A common solution to this problem is to perform a set of calibration measurements with a known source and at varying focal planes [1, 2]. From these measurements and an accurate model for the propagation of the light emitted by the source to the camera, the aberrations can be estimated through phase retrieval algorithms. Initially, only scalar models with point sources were used which allowed the successful use of both iterative and nonlinear optimization routines for estimating the aberrations [1–3]. However, more accurate models [4, 5] take into account the vectorial nature of light which is essential to describe the propagation of the emitted radiation through the interface between the suspension medium and the immersion liquid used for the high-NA microscope objective [6]. Moreover, it is also necessary to consider that the most common sources, such as fluorescent nanobeads, emit incoherent light and their size can thus lead to a noticable blurring of the PSFs. Given these more accurate assumptions, iterative algortihms cannot be directly applied and have to be adapted which can make them ustable, although some succes has been demostrated [4]. A more natural appproach is to use nonlinear optimization [5, 7] since it provides us with the freedom to incorporate othe unknown parameters into the estimation, such as the photobleaching amplitudes or the background illumination.

Up until now, all works have assumed a scalar pupil to characterize the aberrations or to design new PSFs. However, SMOLM requires the use of birefringent elements to encode the orientation information of the emitting dipole into the shape of the two polarization components of the PSF. Therefore, it is important to update the model of propagation for an accurate characterization or design of SMOLM systems. In this work, we propose a characterization technique and algorithm to estimate the polarization aberrations of the sytem [8] as well as other unknown (or poorly known) parameters. This is done by applying a nonlinear optimization algorithm to a physical model where the aberrations (or widow we want to design) are now represented by a Jones matrix. The implementation is done with the neural network framework `PyTorch` [] which performs automatically all the gradient computation []. Additionally, we show that, in general, it is necessary to introduce polarization diversity in the measurements in order to properly characterize the polarization response. This is similar to the introduction of phase diversity by taking images at various focal planes. Additionally, we implement the most usful method for taking into account the blurring to the size of the nanobead discussed in []. It should also be noted that all the results obtained in this work were achieved with the software `torchPSFstack` which is freely accesible at [].

II. MODELING THE PSFS FOR FLUORESCENCE MICROSCOPY

A. Field at the back-focal plane

The first step is to have the most accurate model for the propagation of light through our microscope. As shown in Fig. 1, the source is embedded in a medium of index of refraction n_i at a distance $d_{cs} > 0$ from the interface with immersion oil of index of refraction n_f, the interface is given by the coverslip wihch is assumed to be index matched to the immersion oil. For a dipolar source, the green tensor at the back-focal plane (BFP) of a high-NA objective can be computed by decompositing the using Richards-Wolf diffraction theory for an aplanatic systems [6**?**]. An important step in this calculation is to take into account the interface between the two media since it introduces spherical aberration and the coupling of evanescent waves when $n_f > n_i$, known as supercritical angle fluorescence (SAF), which can contribute to more than half of the radiation reaching the detector [9–11].

Following [6, 12] and assuming that light propagates along the positive $\hat{z}$ direction, the Green tensor at the

* rodrigo.gutierrez-cuevas@fresnel.fr

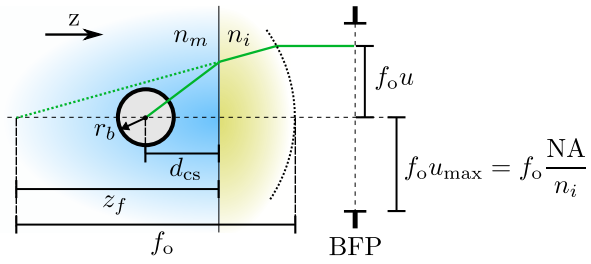

FIG. 1. .

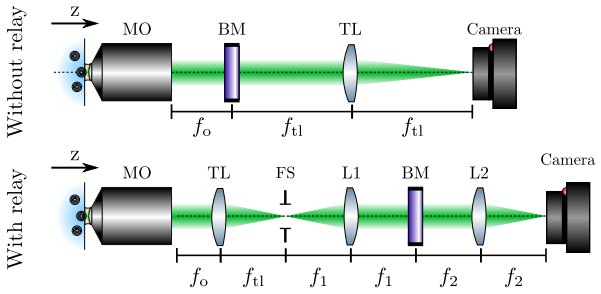

FIG. 2. .

BFP,

$$\mathbf{G}_0(\mathbf{u}) = e^{-ikn_i\boldsymbol{\rho}_o\cdot\mathbf{u}} \exp\left[ikn_m d_{cs}\sqrt{1-\left(\frac{n_i u}{n_m}\right)^2}\right] \times \exp\left(ikn_i z_f\sqrt{1-u^2}\right)\mathbf{g}(\mathbf{u}), \quad (1)$$

where

$$\mathbf{g}(\mathbf{u}) = \begin{pmatrix} g_{xx}(\mathbf{u}) & g_{xy}(\mathbf{u}) & g_{xz}(\mathbf{u}) \\ g_{yx}(\mathbf{u}) & g_{yy}(\mathbf{u}) & g_{yz}(\mathbf{u}) \end{pmatrix} \quad (2)$$

with the explicit form of its components given in the Appendix, $\boldsymbol{\rho}_o = (x_o, y_o)$ denotes the transverse location of the dipole, and z_f is the location of the focal plane from the interface, $z_f < 0$ ($z_f > 0$) if the focal plane is in the medium with index of refraction n_i (n_f). The vector $\mathbf{u} = (u_x, u_y)$ denotes the normalized coordinates at the BFP, see Fig. 1. The maximum value of $u = \|\mathbf{u}\|$ is limited by the NA through $u_{max} = \mathrm{NA}/n_i$. The matrix elements g_{ij} include the effect of the Fresnel coefficients of the boundary and depend on $\mathbf{u}$ but not on the location of the dipole or the focal plane. For a dipole oriented along the unit vector $\boldsymbol{\mu} = (\mu_x, \mu_y, \mu_z)$, the electric field distribution at the BFP is given by

$$\mathbf{E}_0(\mathbf{u}) = \mathbf{g}(\mathbf{u};\mathbf{r}_0)\cdot\boldsymbol{\mu}. \quad (3)$$

Therefore, the three columns of the Green tensor represent the field distribution produced by a dipole along each of the three coordinate axes.

B. Propagation from the BFP to the image plane

In order to encode information about the position and orientation of the dipole into the shape of the PSF, it is necessary to include a mask into the path of the emitted light at the BFP with the possible help a relay system as shown in Fig. 2. The most general case is that of a birefringent mask represented by a 2×2 Jones matrix [],

$$\mathbf{J}_M(\mathbf{u}) = \begin{pmatrix} J_{xx} & J_{xy} \\ J_{yx} & J_{yy} \end{pmatrix}. \quad (4)$$

Note that a scalar mask case with apodization is regained if $q_j = 0$ for $j = 1,2,3$, and a pure phase mask if also $q_0 = 1$. After multiplying the Green tensor by this Jones matrix, the field can then be propagated form the BFP to the image plane through

$$\mathbf{G}_{IP}(\boldsymbol{\rho}) = \iint \mathbf{J}_M(\mathbf{u})\cdot\mathbf{G}_0(\pm\mathbf{u})e^{-ik\frac{n_f\boldsymbol{\rho}}{M}\cdot\mathbf{u}}d\mathbf{u}, \quad (5)$$

where M is the total magnification of the system. Note that the normalized coordinate is defined at the location of the birefringent mask. Assuming an incoherent source, the PSF is then given by

$$I_{IP}(\boldsymbol{\rho}) = \|\mathbf{G}_{IP}\|^2 = \sum_{i=x,y}\sum_{j=x,y,z}|G_{IP,ij}(\mathbf{u})|^2. \quad (6)$$

III. MODELING FOR THE PHASE RETRIEVAL

A. Polarization aberrations

The decomposition of polarization aberrations by a Jones matrix can be done in the following manner

$$\mathbf{J}_A(\mathbf{u}) = e^{i2\pi W(\mathbf{u})}\begin{pmatrix} q_0(\mathbf{u})+iq_3(\mathbf{u}) & q_2(\mathbf{u})+iq_1(\mathbf{u}) \\ -q_2(\mathbf{u})+iq_1(\mathbf{u}) & q_0(\mathbf{u})-iq_3(\mathbf{u}) \end{pmatrix}, \quad (7)$$

which allows separating the scalar aberrations, contained in W from the vectorial correction given by the q's. Since aberrations tend to be described by smooth functions, it generally sufices to decompose the various elements of the Jone matrix using the Zernike polynomials which consititute a complete basis on the unit disk. Therefore, we write

$$W(\mathbf{u}) = {\sum_l}' c_l^{(W)} Z_l(\mathbf{u}/u_{max}), \quad (8)$$

$$q_j(\mathbf{u}) = \sum_l c_l^{(j)} Z_l(\mathbf{u}/u_{max}), \quad (9)$$

where $j = 0,...,3$, and we used a single index notation for the basis. Note that $\sum'$ in the expression for W indicates that the terms corresponding to piston and defocus should be excluded, this is automatically handled by the software []. The piston term only fixes a global phase which cannot be determined from intensity

measurements while the defocus term is redundant with the more accurate defocus parameter z_f in Eq. 1. This Zernike expansion is inspired by the Nijboer-Zernike theory [13–15] where a scalar mask would be separated into real and imaginary parts before decomposing in terms of Zernike polynomials. Note that other models can be used, such as pixel by pixel decomposition, but a Zernike decomposition with enough terms should be able to handle most cases found in microscopes. Moreover, computationally there is no advantage to considering a pixel decomposition since the number of DFT (the most costly operation) would be the same. It should also be noted that a scalar mask can easily be modeled by just setting the coefficients $c_l^{(j)} = 0$ for all l and $j = 1, 2, 3$.

B. Best focus and the distance to the coverslip

In general the position chosen as the nominal focus (or best focus) z_f and distance to the coverslip of the emitter d_{cs} are not perfectly known. Therfore, it is worth considering them as part of the optimization parameters that will be estimated along with the coefficients of the Zernike decompositions of the birefringent mask. The most obvious soluttion is to directly use z_f and d_{textcs} as parameters, however both phase terms have similar effect when the radial coordinate u is below the SAF radiation and this might cause the nonlinear optimization to fall into a local minimum which does not provide the real values. Moreover, the estimation of the distance of the best focus z_f will generally depend on the distance of the nanobead from the coverslip. For example, if the paraxial approximation is used then the distance to the best focus will be $z_f = -n_i d_{\text{cs}}/n_m$. A similar result will hold even if we consider the spherical aberration induced by the interface, the only thing that changes is the factor in front of d_{cs}. Therefore, it is best to consider instead

$$\mathbf{G}_0(\mathbf{u}) = D_{\delta,\alpha}(\mathbf{u})\mathbf{g}_0(\mathbf{u}), \tag{10}$$

where

$$D_{\delta,\alpha}(\mathbf{u}) = \exp\left\{\mathrm{i}2\pi n_i\delta\left[\frac{n_m}{n_i}\sqrt{1-\left(\frac{n_i u}{n_m}\right)^2} - \alpha\sqrt{1-u^2}\right]\right\}, \tag{11}$$

with $\delta = d_{\text{cs}}/\lambda$ and $z_f = -\alpha d_{\text{cs}}$. Note that it has been assumed that the source is placed along the optical axis so that $\boldsymbol{\rho}_0 = (0, 0)$. Any deviation from this assumption will be corrected be the scalar tilts given by the tilt Zernike polynomials in the phase term W of $\mathbf{J}_A$. The parameter δ now predominantly controls the amount of exponential decay for the SAF radiation while α controls the defocus of the system. For fluorescing nanobead samples it is safe to assume that they are all fixed to the coverslip so that their distance to the coverslip can be taken as their radius and can be taken off the optimization routine. However, the choice of the best focus is quite subjective and should therefore always be included.

C. Phase and polarization diversity

In phase retrieval algorithms for optical microscopes, it is common practice to assume that we have access to a stack of intensity images at varying focal distances separated by Δz_ζ from the location of the best focus. This varying focal distances are taken into account by multiplying the Green tensor by the phase factor

$$D^\zeta(\mathbf{u}) = \exp\left[\mathrm{i}kn_i\Delta z_\zeta\sqrt{1-u^2}\right] \tag{12}$$

This additional information, referred to as phase diversity, helps the algorithm converge to an appropriate solution without falling into local minima and helps discriminate between the right and left phase vortices. These measurments are sufficient when the aberrations are taken as scalar, however when birefringence effects need to be taken into account it is necessary to implement a method to also provides information about the polarization state of the PSFs for each focal distance. This supplementary information can be obtained by inserting a polarization analyzer right after the birefringence mask (see Fig. 2). This polarization analyzer can be composed of a combination of waveplates and polarizers where at least one elemnt can rotate in order to change the polarization projection of the output. This polarization diversity is modeled by a set of constant Jones matrices $\mathbf{P}^{(p)}$ that is applied after all other birefringent masks. Therefore, the stack of Green tensors at the BFP is given by

$$\mathbf{G}_{\text{BFP}}^{(\zeta,p)}(\mathbf{u}) = D^{(\zeta)}(\mathbf{u})\mathbf{P}^{(p)} \cdot \mathbf{J}_{\text{A}}(\mathbf{u}) \cdot \mathbf{J}_{\text{M}}(\mathbf{u}) \cdot \mathbf{G}_0(\mathbf{u}). \tag{13}$$

In this model $\mathbf{J}_{\text{M}}$ represents any known birefringent mask into the nominal Green tensor which can have approximatly known parameters that can be incorporated into the optimization routine. It is worth noting that while experimentlly the polarization diversity happens at the BFP, computationally it is better to perform it at the image plane in order to avoid the computation of unecessary DFTs.

D. Modeling the total measured intensity

To model the intensity measured by the camera, the Green tensor is first propagated to the image plane via,

$$\mathbf{G}_{\text{IP}}^{(\zeta,p)}(\boldsymbol{\rho}) = \iint \mathbf{G}_{\text{BFP}}^{(\zeta,p)}(\mathbf{u})e^{-\mathrm{i}k\frac{n_i\boldsymbol{\rho}}{M}\cdot\mathbf{u}}\mathrm{d}\mathbf{u}. \tag{14}$$

Here, it will be assumed that the source emits fully unpolarized light. This os the case for fluorescing nanobeads which are commonly used to characterize or test fluorescence microscopes since they have a stronger signal than

that emitted by single fluorescing molecules. In this case the measured intensity is given by the incoherent sum of the PSFs produced by dipoles oriented along each of the three Cartesian axes which is the same as the squared Frobenius norm of the Green tensor at the image plane

$$I_{\mathrm{IP}}^{(\zeta,p)}(\boldsymbol{\rho}) = \left\| \mathbf{G}_{\mathrm{IP}}^{(\zeta,p)} \right\|^2 = \sum_{i=x,y} \sum_{j=x,y,z} |G_{\mathrm{IP,ij}}^{(\zeta,p)}(\mathbf{u})|^2. \quad (15)$$

Depending on the size of the nano-particle it might be necessary to perform one of the blurring operations described in []. If a three-dimensional blurring is needed the computation of supplementary quantities will need to added to the forward model, for example, for the exact hard-sphere model we would also need to compute the total intensity for other values of $d_c s$. The downside is that this would slow the algorithm considerably. However, as long as their diameter is smaller than 30nm one can safely skip this step.

As a last step for computing th emeasured intensity, we also consider the effect of photobleaching of the fluorescing nanobeads and the background illumination. The photobleaching causes the number of photons emitted by the nanobead to diminish with time. Its effect can be taken into account by implementing an overall amplitude factor $\mathcal{A}^{(p,\zeta)}$ which depends on both the phase and polarization diversities. The background illumination is then added incoherently to the photobleached PSF stack. The simplest model is to assume that the background illumination is constant across each intensity image and determined by the term $\mathcal{B}^{(p,\zeta)}$. Therefore, the final total measured intensities of the ZP stack are given by

$$I_{\mathrm{tot}}^{(\zeta,p)}(\boldsymbol{\rho}) = \mathcal{A}^{(p,\zeta)} I_{\mathrm{IP}}^{(\zeta,p)}(\boldsymbol{\rho}) + \mathcal{B}^{(p,\zeta)}. \quad (16)$$

It is possible to assume a more complicated model for the background illumination, such as a quadratic expansion [16].

E. Cost function

This modeled ZP stack of intensity images is then compared to the measured ZP stack $I_{\mathrm{E}}^{(\zeta,p)}$ through a cost function.

IV. NUMERICAL IMPLEMENTATION OF THE PHASE RETRIEVAL

A. Forward model

In order to implement the phase retrieval algorithm, it is necessary to perform all the calculations numerically. Therefore, it will be assumed that all the spatially dependent quantities are sampled in a consistent manner with the pixel pitch of the camera. This two-dimensional sampling will be labeled with a lexicographic index $\boldsymbol{\ell}$ which will take over the spatial dependence on $\mathbf{u}$ and $\boldsymbol{\rho}$, for instance $\mathbf{G}_{\mathrm{J}}(\mathbf{u}) \to \mathbf{G}_{\mathrm{J}}(\boldsymbol{\ell})$. The propagation integral will be computed through fast Fourier transformations denoted by DFT and defined through the one-dimensional kernel $\exp(-\mathrm{i}2\pi\ell'\ell/L)/L$ where L is the total number of points. Its inverse is denoted by IDFT and defined by the kernel $\exp(-\mathrm{i}2\pi\ell'\ell/L)/L^{1/2}$.

Assuming that only the Zernike decomposition coefficients are being optimized over then the forward model can be simply written as:

1. Compute the amplitude and phase or real and imaginary parts of the Pauli coefficients

$$A_0^{(A,P)}(\boldsymbol{\ell}) = \sum_l c_{0,l}^{(A,P)} Z_l(\boldsymbol{\ell}),$$
$$A_j^{(R,I)}(\boldsymbol{\ell}) = \sum_l c_{j,l}^{(R,I)} Z_l(\boldsymbol{\ell}),$$

2. Compute the Pauli components

$$A_0(\boldsymbol{\ell}) = A_0^{(A)}(\boldsymbol{\ell}) e^{\mathrm{i}2\pi A_0^{(P)}(\boldsymbol{\ell})},$$
$$A_j(\boldsymbol{\ell}) = A_j^{(R)}(\boldsymbol{\ell}) + \mathrm{i} A_j^{(I)}(\boldsymbol{\ell}).$$

3. Compute the Jones matrix of the aberrations

$$\mathbf{J}_{\mathrm{A}}(\boldsymbol{\ell}) = \begin{pmatrix} A_0(\boldsymbol{\ell}) + A_1(\boldsymbol{\ell}) & A_2(\boldsymbol{\ell}) - \mathrm{i}A_3(\boldsymbol{\ell}) \\ A_2(\boldsymbol{\ell}) + \mathrm{i}A_3(\boldsymbol{\ell}) & A_0(\boldsymbol{\ell}) - A_1(\boldsymbol{\ell}) \end{pmatrix}.$$

4. Compute the Green tensor at the BFP

$$\mathbf{G}_{\mathrm{BFP}}(\boldsymbol{\ell}) = \mathbf{J}_{\mathrm{A}}(\boldsymbol{\ell}) \cdot \mathbf{G}_{\mathrm{J}}(\boldsymbol{\ell}).$$

5. Include the phase diversity in the Green tensor at the BFP but *not* the polarization diversity

$$\mathbf{G}_{\mathrm{BFP}}^{(\zeta)}(\boldsymbol{\ell}) = D^{(\zeta)}(\boldsymbol{\ell}) \mathbf{G}_{\mathrm{BFP}}(\boldsymbol{\ell}).$$

6. Propagate to the image plane

$$\mathbf{G}_{\mathrm{IP}}^{(\zeta)}(\boldsymbol{\ell}) = \mathrm{DFT}\{\mathbf{G}_{\mathrm{J}}(\boldsymbol{\ell}')\}.$$

7. Propagate through the polarization analyzer

$$\mathbf{G}_{\mathrm{IP}}^{(\zeta,p)}(\boldsymbol{\ell}) = \mathbf{P}^{(p)} \cdot \mathbf{G}_{\mathrm{IP}}^{(\zeta)}(\boldsymbol{\ell}).$$

8. Compute the intensity

$$I_{\mathrm{IP}}^{(\zeta,p)}(\boldsymbol{\ell}) = \sum_{i=x,y} \sum_{j=x,y,z} |G_{\mathrm{IP,ij}}^{(\zeta,p)}(\boldsymbol{\ell})|^2.$$

9. Take into account the photobleaching and the background illumination

$$I_{\mathrm{tot}}^{(\zeta,p)}(\boldsymbol{\ell}) = \mathcal{A}^{(p,\zeta)} I_{\mathrm{IP}}^{(\zeta,p)}(\boldsymbol{\ell}) + \mathcal{B}^{(p,\zeta)}.$$

10. Compute the cost function by masking with $w(\boldsymbol{\ell})$ bad pixels or computed points that are outside of those provided by the measured intensities

$$\mathcal{C}_{\rm SD} = \sum_{\zeta,p}\sum_{\boldsymbol{\ell}} w(\boldsymbol{\ell})\left[I_{\rm E}^{(\zeta,p)}(\boldsymbol{\ell}) - I_{\rm tot}^{(\zeta,p)}(\boldsymbol{\ell})\right]^2 \quad \text{or}$$

$$\mathcal{C}_{\rm LL} = -\sum_{\zeta,p}\sum_{\boldsymbol{\ell}} w(\boldsymbol{\ell})\left\{I_{\rm E}^{(\zeta,p)}(\boldsymbol{\ell})\ln\left[I_{\rm tot}^{(\zeta,p)}(\boldsymbol{\ell})\right] - I_{\rm tot}^{(\zeta,p)}(\boldsymbol{\ell})\right\}.$$

In the last step, the two most common choices for the cost function were introduced. The first, $\mathcal{C}_{\rm SD}$, is the sum of the squared difference between the modeled and measured ZP stacks. This cost function is well-suited when the noise follows a Gaussian distribution. However, for fluorescence microscopy given the low number of incident photons, the noise follows a Poisson distribution. In this case the log-likelihood cost function $\mathcal{C}_{\rm LL}$ is more appropriate. It is worth making a technical note at this point. In order for the Poisson distribution to work best we need to work with the data that follows a Poisson distribution which means that the noise in the measured data should not be removed, and the offset specific to the camera should have been removed.

B. Extra parameters

As was already discussed, in experimental settings it often happens that some values can only be approximately known. The advantage of the nonlinear optimization approach to phase retrieval is that these parameters can also be estimated. These include the δ and α parameters introduced earlier, but also the photobleaching amplitudes $\mathcal{A}^{(p,\zeta)}$ and the background illumination $\mathcal{B}^{(p,\zeta)}$. Moreover, the modular form of the forward model and the gradient computation greatly simplifies their inclusion. Depending on how the particular parameter enters the forward model it might be necessary to add a parallel branch which merges with the main one presented in the previous section. But in every case, it will be necessary branch out the backward model in order to perform the gradient computation.

Given that the forward and backward models can be easily identified by the absence or presence of an overbar in the left hand side term, we only need a nomenclature to identify the various branches. For this, a letter following the step number will be used with the same letter being used for the forward and backward models. Furthermore, we assume there is an implicit letter "a" following the step numbers of the main branch.

For the δ and α parameters the merging in the forward model occurs at step 4 since they are already included in the term $\mathbf{G}_{\rm J}(\boldsymbol{\ell})$.

1b. Compute the complex argument of the exponential term containing the defocus and SAF terms

$$S_{\delta,\alpha}(\boldsymbol{\ell}) = {\rm i}2\pi n_i\delta\left[\frac{n_m}{n_i}\sqrt{1-\left(\frac{n_i u(\boldsymbol{\ell})}{n_m}\right)^2} - \alpha\sqrt{1-u^2(\boldsymbol{\ell})}\right],$$

2b. Compute the exponential

$$D_{\delta,\alpha}(\boldsymbol{\ell}) = e^{S_{\delta,\alpha}(\boldsymbol{\ell})}.$$

3b. Compute the Green tensor including the birefringent mask, the defocus and SAF terms

$$\mathbf{G}_{\rm J}(\boldsymbol{\ell}) = D_{\delta,\alpha}(\boldsymbol{\ell})\mathbf{g}_{\rm J}(\boldsymbol{\ell}).$$

V. IMPLEMENTATION OF THE PHASE RETRIEVAL ALGORITHM

A. Initial considerations

To exemplify the implementation of the phase retrieval algorithm, let us consider the setup used for CHIDO. In this case the birefringent window is composed of a stress engineered optical (SEO) element followed by a quarter-wave plate at 45°. Afterwards, the light is separated into its x and y linear polarization components with a Wollaston prism which are then measured by the camera. This same setup can be used to obtain the necessary ZP stack for the phase retrieval algorithm by taking the SEO as the birefringent mask given by the Jones matrix

$$\mathbf{J}_{\rm SEO}(\mathbf{u}) = \cos\frac{cu}{2}\begin{pmatrix}1&0\\0&1\end{pmatrix} + {\rm i}\sin\frac{cu}{2}\begin{pmatrix}\cos\phi&-\sin\phi\\\sin\phi&-\cos\phi\end{pmatrix}, \tag{17}$$

and the quarter-wave plate along with the Wollaston as the polarization analyzer. To increase the number of polarization diversities, the quarter-wave plate will be allowed to be placed at various angles. This combination defines the polarization diversity Jones matrices through

$$\mathbf{P}^{(p)} = \left\{\begin{pmatrix}1&0\\0&0\end{pmatrix}\right\}\cdot\begin{pmatrix}\cos^2\theta_p + i\sin^2\theta_p & (1-i)\sin\theta_p\cos\theta_p\\(1-i)\sin\theta_p\cos\theta_p & \sin^2\theta_p + i\cos^2\theta_p\end{pmatrix} \tag{18}$$
$$\left\{\begin{pmatrix}0&0\\0&1\end{pmatrix}\right\}$$

where θ_p is the angle of the fast axis with respect to the x axis. Having defined the polarization diversity, the ZP stack can be acquired by taking images of the PSFs for all the polarization diversity at various focal planes. Note that before using these images for the retrieval of the aberrations and the other parameters, they need to be processed so that they follow the assumed statistics. This is done by converting the value at each pixel from the arbitrary gray scale value to the number of photocount events. In most cases, an offset value needs to be removed (if any pixel has a negative value then it should be set to zero), and then the gray value should be converted to the number of photoelectrons.

Before being able to launch the phase retrieval, all the parameters that are going to be estimated need to be provided with an initial value. For the Zernike coefficients, the simplest choice is to set all equal to zero except the first coefficient of $A_0(A)$ which reduces the aberration matrix to the identity.

Depending on the particular type of sample used for acquiring the ZPstack, the distance to the coverslip might be estimated. For example, if the emitters are fixed at the surface of the coverslip then $d_{\rm cs}$ is equal to the radius of the nanobead or if they are attached to a macro sphere, $d_{\rm cs}$ can be estimated by the radial distance of the emitter from the center of the macrosphere. When $d_{\rm cs}$ cannot be estimated from the sample, if the setup allows imaging the pupil $d_{\rm cs}$ can be estimated from the exponential decay of the SAF radiation. Otherwise, an initial value not much greater to the nanobead's radius should work fine.

For the parameter setting the distance of the best focus in terms of $d_{\rm cs}$ there are several options. If, experimentally, there is a particular criteria to choose the best focus, e.g. the smallest rms width of the PSFs, then the same one could be used to define it. However, if the best focus is defined experimentally "by eye" then there are several sensible options, such as the parameter that sets the second derivative of the defocus and SAF wavefront equal to zero or that the average of the first derivative is zero. It should be noted that in general this parameter should be greater than the one used for the paraxial focus sin the PSF quickly degrades as we move away from and closer to the coverslip but not when we move to the other side.

The background illumination can be estimated directly form the images in the experimental ZP stack by averaging the pixels in the corners of each PSF image or in an empty region close to the nanobead being analyzed. Finally for the phobleaching coefficients, they could all be set equal to zero if the effect is negligible. Otherwise, they can be estimated numerically computing the PSFs, setting the scale of the computed PSFs so that the intensity of one of them is equal to the corresponding experimental image (the calculations should either include the background or it should be removed for the data just for his step), and then setting the photobleaching amplitudes equal to the ratio between the total intensity of the data and the modeled PSFs.

As a lost point, it should be mentioned that the Jones matrix of the birefringent mask should be well characterized. In the case being treated here, this means that the radial parameter c and the orientation set by the angle ϕ_0 are known. They are measured from images of the pupil. Note that, if one desires, this parameters could be added to the phase retrieval algorithm by adding another branch in the forward and backward models.

VI. ALTERNATIVE DECOMPOSITION FOR THE ABERRATION MATRIX

A. Unitary decomposition

Another useful decomposition for the aberration Jones matrix is based on the assumption that the aberrations mostly conserve energy. Thus the aberration matrix can be written as

$$\begin{aligned}\mathbf{J}_{\rm A}(\mathbf{u}) =& A(\mathbf{u})e^{{\rm i}2\pi W(\mathbf{u})}\left[q_0(\mathbf{u})\boldsymbol{\sigma}_0 + {\rm i}\sum_{j=1}^{3} q_j(\mathbf{u})\boldsymbol{\sigma}_j\right]\\ =& A(\mathbf{u})e^{{\rm i}2\pi W(\mathbf{u})}\\ &\times\begin{pmatrix} q_0(\mathbf{u})+{\rm i}q_3(\mathbf{u}) & q_2(\mathbf{u})+{\rm i}q_1(\mathbf{u})\\ -q_2(\mathbf{u})+{\rm i}q_1(\mathbf{u}) & q_0(\mathbf{u})-{\rm i}q_3(\mathbf{u})\end{pmatrix},\end{aligned}$$

which is a unitary matrix if we set

$$q_0(\mathbf{u}) = \sqrt{1-\sum_{j=1}^{3} q_j^2(\mathbf{u})}, \tag{19}$$

and for which the total transmission can vary through the amplitude term $A(\mathbf{u})$. This decomposition is equivalent to considering another birefringent mask followed by a scalar one.

In this case, the amplitude A, the phase Φ, and the coefficients q_j will be assumed to be real. This allows the implementation of unitary birefringent masks. Expanding them in terms of the Zernike polynomials,

$$A(\mathbf{u}) = \sum_l c_l^{(A)} Z_l(\mathbf{u}/u_{\max}), \tag{20}$$

$$W(\mathbf{u}) = \sum_l c_l^{(W)} Z_l(\mathbf{u}/u_{\max}), \tag{21}$$

$$q_j(\mathbf{u}) = \sum_l c_l^{(j)} Z_l(\mathbf{u}/u_{\max}), \tag{22}$$

where we used the single index notation for the basis. In the decomposition of Φ the Zernike polynomials corresponding to piston and defocus are again dropped. Note that the q_0 parameter is then fixed by the others through the unitarity condition.

B. Forward model

Given that these changes only affect the computation of the Jones matrix for the aberrations, only the steps 1 through 3 of the branch "a" need to be changed by

1. Compute the amplitude, phase and q_j coefficients

$$A(\boldsymbol{\ell}) = \sum_l c_l^{(A)} Z_l(\boldsymbol{\ell}),$$

$$W(\boldsymbol{\ell}) = \sum_l c_l^{(W)} Z_l(\boldsymbol{\ell}),$$

$$q_j(\boldsymbol{\ell}) = \sum_l c_l^{(j)} Z_l(\boldsymbol{\ell}).$$

2. Compute the scalar and matrix parts

$$\begin{aligned}\Gamma(\boldsymbol{\ell}) =& A(\boldsymbol{\ell}) e^{\mathrm{i}2\pi W(\boldsymbol{\ell})},\\ \mathbf{Q}(\boldsymbol{\ell}) =& \begin{pmatrix} q_0(\boldsymbol{\ell}) + \mathrm{i}q_3(\boldsymbol{\ell}) & q_2(\boldsymbol{\ell}) + \mathrm{i}q_1(\boldsymbol{\ell}) \\ -q_2(\boldsymbol{\ell}) + \mathrm{i}q_1(\boldsymbol{\ell}) & q_0(\boldsymbol{\ell}) - \mathrm{i}q_3(\boldsymbol{\ell}) \end{pmatrix},\end{aligned}$$

where

$$q_0(\boldsymbol{\ell}) = \sqrt{1 - \sum_{j=1}^{3} q_j^2(\boldsymbol{\ell})}.$$

3. Compute the Jones matrix of the aberrations

$$\mathbf{J}_\mathrm{A}(\boldsymbol{\ell}) = \Gamma(\boldsymbol{\ell})\mathbf{Q}(\boldsymbol{\ell}).$$

C. Gradient computations

The changes of the forward model need to be accompanied by changes in the gradient computation. Steps 8 to 10 of the main branch "a" need to be substituted by

8. Gradient with respect to the Pauli expansion coefficients

$$\begin{aligned}\bar{\Gamma}(\boldsymbol{\ell}) =& \sum_{i,j=x,y} Q_{ij}^*(\boldsymbol{\ell}) \bar{J}_{A,ij}(\boldsymbol{\ell}),\\ \bar{\mathbf{Q}}(\boldsymbol{\ell}) =& \Gamma^*(\boldsymbol{\ell}) \bar{\mathbf{J}}_A(\boldsymbol{\ell}).\end{aligned}$$

9. Gradient with respect to the amplitude and phase or real and imaginary parts of the Pauli coefficients

$$\begin{aligned}\bar{A}(\boldsymbol{\ell}) =& \mathrm{Re}\left\{\bar{\Gamma}(\boldsymbol{\ell}) \exp\left[-\mathrm{i}2\pi \sum_l c_l^{(W)} Z_l(\boldsymbol{\ell})\right]\right\},\\ \bar{W}(\boldsymbol{\ell}) =& 2\pi \mathrm{Im}\left\{\bar{\Gamma}(\boldsymbol{\ell})\Gamma^*(\boldsymbol{\ell})\right\},\\ \bar{q}_1(\boldsymbol{\ell}) =& \mathrm{Im}\left\{\bar{Q}_{x,y}(\boldsymbol{\ell}) + \bar{Q}_{y,x}(\boldsymbol{\ell})\right\} - \frac{\bar{q}_0(\boldsymbol{\ell})}{q_0(\boldsymbol{\ell})} q_1(\boldsymbol{\ell}),\\ \bar{q}_2(\boldsymbol{\ell}) =& \mathrm{Re}\left\{\bar{Q}_{x,y}(\boldsymbol{\ell}) - \bar{Q}_{y,x}(\boldsymbol{\ell})\right\} - \frac{\bar{q}_0(\boldsymbol{\ell})}{q_0(\boldsymbol{\ell})} q_2(\boldsymbol{\ell}),\\ \bar{q}_3(\boldsymbol{\ell}) =& \mathrm{Im}\left\{\bar{Q}_{x,x}(\boldsymbol{\ell}) - \bar{Q}_{y,y}(\boldsymbol{\ell})\right\} - \frac{\bar{q}_0(\boldsymbol{\ell})}{q_0(\boldsymbol{\ell})} q_3(\boldsymbol{\ell}).\end{aligned}$$

where

$$\bar{q}_0(\boldsymbol{\ell}) = \mathrm{Re}\left\{\bar{Q}_{x,x}(\boldsymbol{\ell}) + \bar{Q}_{y,y}(\boldsymbol{\ell})\right\}.$$

10. Gradient with respect to the Zernike expansion coefficients

$$\begin{aligned}\bar{c}^{(A)} =& \sum_{\boldsymbol{\ell}} \bar{A}(\boldsymbol{\ell}) Z_l(\boldsymbol{\ell}),\\ \bar{c}_l^{(W)} =& \sum_{\boldsymbol{\ell}} \bar{W}(\boldsymbol{\ell}) Z_l(\boldsymbol{\ell}),\\ \bar{c}_l^{(j)} =& \sum_{\boldsymbol{\ell}} \bar{q}_j(\boldsymbol{\ell}) Z_l(\boldsymbol{\ell}).\end{aligned}$$

ACKNOWLEDGMENTS

S. Paine for useful discussions.

Appendix A: Expressions for the Green tensor at the BFP

As outlined in [6], a closed-form for the Green tensor at the BFP for a dipolar source placed close to an interface can be obtained. In particular the components of the **g** tensor in Eq. (**??**) are given by

$$\mathbf{g}(\mathbf{u}) = \frac{1}{(1-u^2)^{1/4}} \begin{pmatrix} \cos^2\phi\sqrt{1-u^2}\Phi_2 + \sin^2\phi\Phi_3 & \cos\phi\sin\phi(\sqrt{1-u^2}\Phi_2 - \Phi_3) & -u\cos\phi\Phi_1 \\ \cos\phi\sin\phi(\sqrt{1-u^2}\Phi_2 - \Phi_3) & \sin^2\phi\sqrt{1-u^2}\Phi_2 + \cos^2\phi\Phi_3 & -u\sin\phi\Phi_1 \end{pmatrix}. \tag{A1}$$

where

$$\Phi_1(u) = t^p(u) \frac{n_i k_i \sqrt{1-u^2}}{n_m \sqrt{k_m^2 - k_i^2 u^2}} \tag{A2a}$$

$$\Phi_2(u) = t^p(u) \frac{n_i}{n_m} \tag{A2b}$$

$$\Phi_3(u) = t^s(u) \frac{k_i \sqrt{1-u^2}}{\sqrt{k_m^2 - k_i^2 u^2}} \tag{A2c}$$

with

$$t^s(u) = \frac{2k_{m,z}}{k_{m,z} + k_{i,z}}, \tag{A3a}$$

$$t^p(u) = \frac{n_m}{n_i} \frac{2n_i^2 k_{m,z}}{n_i^2 k_{m,z} + n_m^2 k_{i,z}}. \tag{A3b}$$

being the Fresnel coefficients for p and s polarized light.

[1] B. M. Hanser, M. G. L. Gustafsson, D. A. Agard, and J. W. Sedat, Optics Letters **28**, 801 (2003).

[2] B. M. HANSER, M. G. L. GUSTAFSSON, D. A. AGARD, and J. W. SEDAT, Journal of Microscopy **216**, 32 (2004).

[3] N. A. Clark, *Microscope Characterization using Phase Retrieval Applied to Determine the Spatial Distribution of Membrane-Associated Proteins in Hematocytes*, Ph.D. thesis, University of Rochester (2012).

[4] N. H. Thao, O. Soloviev, and M. Verhaegen, Journal of the Optical Society of America A **37**, 16 (2019).

[5] B. Ferdman, E. Nehme, L. E. Weiss, R. Orange, O. Alalouf, and Y. Shechtman, Optics Express **28**, 10179 (2020).

[6] L. Novotny and B. Hecht, *Principles of Nano-Optics* (Cambridge University Press, 2006).

[7] J. R. Fienup, Applied Optics **21**, 2758 (1982).

[8] E. W. Hansen, in *Polarization Considerations for Optical Systems*, edited by R. A. Chipman (SPIE, 1988).

[9] E. H. Hellen and D. Axelrod, Journal of the Optical Society of America B **4**, 337 (1987).

[10] D. Axelrod, Traffic **2**, 764 (2001).

[11] D. Axelrod, Biophysical Journal **104**, 1401 (2013).

[12] M. A. Lieb, J. M. Zavislan, and L. Novotny, Journal of the Optical Society of America B **21**, 1210 (2004).

[13] A. J. E. M. Janssen, Journal of the Optical Society of America A **19**, 849 (2002).

[14] J. J. M. Braat, P. Dirksen, A. J. E. M. Janssen, and A. S. van de Nes, Journal of the Optical Society of America A **20**, 2281 (2003).

[15] J. J. Braat, P. Dirksen, A. J. Janssen, S. van Haver, and A. S. van de Nes, Journal of the Optical Society of America A **22**, 2635 (2005).

[16] A. Aristov, B. Lelandais, E. Rensen, and C. Zimmer, Nature Communications **9** (2018), 10.1038/s41467-018-04709-4.